ALMA Detection of [O <sc>iii</sc>] 88 μm at z=12.33: Exploring the Nature and Evolution of GHZ2 as a Massive Compact Stellar

The Astrophysical Journal Letters, 977:L9 (9pp), 2024 December 10 https://doi.org/10.3847/2041-8213/ad8f38

ALMA Detection of [O III] 88 μm at $z = 12.33$: Exploring the Nature and Evolution of GHZ2 as a Massive Compact Stellar System

Jorge A. Zavala[1], Tom Bakx[2], Ikki Mitsuhashi[3], Marco Castellano[4], Antonello Calabro[4], Hollis Akins[5], Veronique Buat[6], Caitlin M. Casey[5], David Fernandez-Arenas[7,8], Maximilien Franco[5], Adriano Fontana[9], Bunyo Hatsukade[1,10,11], Luis C. Ho[12,13], Ryota Ikeda[1,14], Jeyhan Kartaltepe[15], Anton M. Koekemoer[16], Jed McKinney[5], Lorenzo Napolitano[9,17], Pablo G. Pérez-González[18], Paola Santini[4], Stephen Serjeant[19], Elena Terlevich[20,21,22], Roberto Terlevich[20,21,22], and L. Y. Aaron Yung[16]

[1] National Astronomical Observatory of Japan, 2-21-1 Osawa, Mitaka, Tokyo 181-8588, Japan
[2] Department of Space, Earth, & Environment, Chalmers University of Technology, Chalmersplatsen 4 412 96 Gothenburg, Sweden
[3] Waseda Research Institute for Science and Engineering, Faculty of Science and Engineering, Waseda University, 3-4-1, Okubo, Shinjuku, Tokyo 169-8555, Japan
[4] INAF—Osservatorio Astronomico di Roma, via di Frascati 33, 00078 Monte Porzio Catone, Italy
[5] Department of Astronomy, The University of Texas at Austin, 2515 Speedway Boulevard Stop C1400, Austin, TX 78712, USA
[6] Aix Marseille Univ, CNRS, CNES, LAM, Marseille, France
[7] Canada–France–Hawaii Telescope, Kamuela, HI 96743, USA
[8] Instituto de Radioastronomía y Astrofísica, UNAM Campus Morelia, Apartado postal 3-72, 58090 Morelia, Michoacán, Mexico
[9] INAF—Osservatorio Astronomico di Roma, Via Frascati 33, 00078, Monte Porzio Catone, Italy
[10] Graduate Institute for Advanced Studies, SOKENDAI, Osawa, Mitaka, Tokyo 181-8588, Japan
[11] Institute of Astronomy, Graduate School of Science, The University of Tokyo, 2-21-1 Osawa, Mitaka, Tokyo 181-0015, Japan
[12] Kavli Institute for Astronomy and Astrophysics, Peking University, Beijing 100871, People's Republic of China
[13] Department of Astronomy, School of Physics, Peking University, Beijing 100871, People's Republic of China
[14] Department of Astronomy, School of Science, SOKENDAI (The Graduate University for Advanced Studies), 2-21-1 Osawa, Mitaka, Tokyo 181-8588, Japan
[15] Laboratory for Multiwavelength Astrophysics, School of Physics and Astronomy, Rochester Institute of Technology, 84 Lomb Memorial Drive, Rochester, NY 14623, USA
[16] Space Telescope Science Institute, 3700 San Martin Drive, Baltimore, MD 21218, USA
[17] Dipartimento di Fisica, Università di Roma Sapienza, Città Universitaria di Roma - Sapienza, Piazzale Aldo Moro, 2, 00185, Roma, Italy
[18] Centro de Astrobiología (CAB), CSIC-INTA, Ctra. de Ajalvir km 4, Torrejón de Ardoz, E-28850, Madrid, Spain
[19] School of Physical Sciences, The Open University, Walton Hall, Milton Keynes, MK7 6AA, UK
[20] Instituto Nacional de Astrofísica, Óptica y Electrónica,Tonantzintla, Puebla, México
[21] Institute of Astronomy, University of Cambridge, Cambridge, CB3 0HA, UK
[22] Facultad de Astronomía y Geofísica, Universidad de La Plata, La Plata, Argentina
Received 2024 October 1; revised 2024 November 1; accepted 2024 November 5; published 2024 December 10

Abstract

We present Atacama Large Millimeter/submillimeter Array observations on the high-redshift galaxy GHZ2 and report a successful detection of the rest-frame 88 μm atomic transition from doubly ionized oxygen at $z = 12.3327 \pm 0.0035$. Based on these observations, combined with additional constraints on the [O III] 52 μm line luminosity and previous JWST data, we argue that GHZ2 is likely powered by compact and young star formation and show that it follows well-established relationships found for giant H II regions and metal-poor star-forming dwarf galaxies that are known to host bright super star clusters. Additionally, these observations provide new constraints on the oxygen electron density ($100 \lesssim n_e\,[\mathrm{cm}^{-3}] \lesssim 4{,}000$) and dynamical mass ($M_{\rm dyn} \approx 3$–$8 \times 10^8\,M_\odot$). The existence of these massive starburst systems 13.3 Gyr ago might explain the origin of today's globular clusters, a long-standing question in astronomy. To test this, we present observational probes to investigate whether sources like GHZ2 are linked to the formation of today's globular clusters or other more massive compact stellar systems.

Unified Astronomy Thesaurus concepts: Galaxy evolution (594); High-redshift galaxies (734); Galaxies (573); Early universe (435); Emission line galaxies (459); Starburst galaxies (1570); Globular star clusters (656); Compact galaxies (285); Young massive clusters (2049); Ultracompact dwarf galaxies (1734); Far infrared astronomy (529); Submillimeter astronomy (1647)

1. Introduction

The discovery of bright galaxies at very high redshifts ($z \gtrsim 10$) by the James Webb Space Telescope (JWST) is challenging our understanding of galaxy formation and evolution. Their high luminosities ($M_{\rm UV} < -20$) and inferred volume density are in tension with the predictions from widely adopted (pre-JWST) theoretical studies (e.g., M. Castellano et al. 2023; S. L. Finkelstein et al. 2023; N. J. Adams et al. 2024; Y. Harikane et al. 2024). This could be the result of very young stellar populations and/or bursty star formation, enhanced star formation efficiencies in the early Universe, contribution from active black holes, or strong evolution in the dust properties, among others, including a nonuniversal initial mass function or modifications to the standard cosmology itself (e.g., B. Liu & V. Bromm 2022; A. Ferrara et al. 2023; M. Boylan-Kolchin 2023; G. Sun et al. 2023; R. Feldmann et al. 2024; S. Hegde et al. 2024; L. Y. A. Yung et al. 2024).

These galaxies thus provide crucial insights into the earliest phases of galaxy formation within the first few hundred million years after the big bang, as well as into the galaxy–dark matter connection and black hole–galaxy coevolution. To date, more

than 10 galaxies have been spectroscopically confirmed at $z > 10$ (see the recent compilation by G. Roberts-Borsani et al. 2024), reaching up to $z \sim 14$ (S. Carniani et al. 2024b), but their nature and primary source of excitation remain unclear, especially for the brightest and most compact systems. Are they primarily powered by intense star formation or do they host active galactic nuclei (AGN) that contribute significantly to their luminosity?

To address this question, spectroscopic observations to probe the physics of their multiphase interstellar media are essential. At high redshifts, the JWST NIRSpec instrument has become one of the workhorses for characterizing these systems thanks to its high sensitivity and wavelength coverage (e.g., P. Arrabal Haro et al. 2023; A. J. Bunker et al. 2023; E. Curtis-Lake et al. 2023; S. Fujimoto et al. 2023; R. L. Sanders et al. 2023; B. Wang et al. 2023), but at $z \gtrsim 9$–10, it provides access mainly to rest-frame UV lines. Recently, the Mid-Infrared Instrument (MIRI) has also been used to study some of the highest-redshift galaxies since it probes the well studied (and typically bright) rest-frame optical emission lines up to $z \gtrsim 14$–15, offering valuable complementary data to the NIRSpec observations (e.g., J. Álvarez-Márquez et al. 2024; T. Y.-Y. Hsiao et al. 2024b; J. A. Zavala et al. 2024). Furthermore, the Atacama Large Millimeter/submillimeter Array (ALMA) is uniquely equipped to characterize high-redshift galaxies through the detection of far-infrared emission lines, which can also serve as powerful diagnostics for the physical conditions of distant galaxies (e.g., A. K. Inoue et al. 2014, 2016; S. Carniani et al. 2017; T. Hashimoto et al. 2019; T. J. L. C. Bakx et al. 2020), specifically when using multiwavelength line diagnostics (e.g., H. Katz et al. 2019; Y. Nakazato et al. 2023).

Nevertheless, some recent ALMA follow-ups on ultra–high-redshift galaxy candidates have resulted in nondetections (T. J. L. C. Bakx et al. 2023; M. Kaasinen et al. 2023; I. Yoon et al. 2023), preventing us from fully characterizing the nature of these systems and calling into question ALMA's capabilities to study the $z \gtrsim 10$ Universe. Most of these observations, however, suffered from targets with highly uncertain redshifts (most of them limited to photometric redshifts), which require line searches through multisetup spectral scans, limiting the sensitivity of the observations and preventing the derivation of tight constraints on their physical properties.

In this study, we present deep ALMA observations targeting a spectroscopically confirmed galaxy within the Universe's first 400 Myr, GHZ2/GLASSz12 at $z = 12.3$ (hereafter GHZ2; M. Castellano et al. 2024; J. A. Zavala et al. 2024; see also M. Castellano et al. 2022; R. P. Naidu et al. 2022; A. Calabro et al. 2024), and report a successful detection of the [O III] 88 μm far-infrared emission line. This breakthrough allows us to place new constraints on the physical properties of this unique galaxy, which stands out as one of the brightest known objects at this epoch ($M_{\rm UV} \approx -20.5$). Moreover, this study provides critical insights into the nature and evolution of the luminous high-redshift galaxies recently discovered by JWST and the mechanisms powering their extraordinary brightness, while demonstrating the feasibility of studying these early systems with ALMA.

The enormous potential of the ALMA–JWST synergy is further demonstrated by S. Carniani et al. (2024a) and S. Schouws et al. (2024), who reported subsequent ALMA observations on a higher-redshift galaxy, JADES-z14-0, with a successful detection of the [O III] 88 μm transition at $z = 14.18$.

This Letter is structured as follows. Section 2 presents the details of the ALMA observations and data reduction, as well as the identification of the [O III] 88 μm line. The main results of the Letter and the comparison of the properties of GHZ2 and those from local and low-redshift star-forming systems are presented in Section 3. In Section 4, we discuss circumstantial evidence relating GHZ2, and other bright high-redshift galaxies, to globular clusters and other compact stellar systems. Finally, a summary of this work is presented in Section 5. A companion paper (I. Mitsuhashi et al. 2024, in preparation) will present the dust constraints inferred from the ALMA continuum observations (undetected at $>3\sigma$).

Throughout this Letter, we assume a flat ΛCDM cosmology with $\Omega_{\rm m} = 0.29$, $\Omega_\Lambda = 0.71$, and $H_0 = 69.6\ {\rm km\ s^{-1}\ Mpc^{-1}}$.

2. ALMA Observations, Data Reduction, and Data Analysis

2.1. Observations and Data Reduction

The source GHZ2 was previously targeted by ALMA using a Band 6 spectral scan strategy to search for the [O III] 88 μm line ($\nu_{\rm rest} = 3393.0062$ GHz) across the frequency range 234–263 GHz, corresponding to $z \approx 11.9$–13.55. Nevertheless, no robust detection was identified at the JWST position of the target (T. J. L. C. Bakx et al. 2023; see also G. Popping 2023). After the spectroscopic redshift confirmation by JWST/NIRSpec and JWST/MIRI (M. Castellano et al. 2024; J. A. Zavala et al. 2024), deeper ALMA observations were obtained in 2024 April around the refined expected frequency of the line at 254.45 GHz as part of the Director's Discretionary Time (DDT) project 2023.A.00017.S (PI: J. Zavala). The new observations consist of ∼4.9 hr on source (∼8.7 hr including calibrations and overheads), which adds to ∼7 hr on source in total when combining the cycle 9 and cycle 10 data sets. Unfortunately, the new data do not cover the previous tentative line reported by T. J. L. C. Bakx et al. (2023) at $\nu = 258.67$ GHz.

Additionally, Band 8 observations covering the redshifted [OIII] 52 μm line ($\nu_{\rm rest} = 5785.8796$ GHz) were also carried out as part of project 2023.A.00017.S. The spectral setup covers the frequency ranges 418.6–422.4 and 430.8 −434.5 GHz, with an on-source time of 2.5 hr (4.8 hr including calibrations and overheads). These observations are by design shallower than the Band 6 data since were only aimed to provide a limit on the [O III] 52 μm in the case of an extreme electron density (see Section 3.3). Matching the Band 6 sensitivity would have required a much larger time investment that is beyond the scope of a DDT proposal.

Data reduction was performed as described in T. J. L. C. Bakx et al. (2023), using CASA and following the standard ALMA pipeline workflow. Then, as part of our imaging process, we created data cubes from the u-v visibilities using a natural weighting to maximize the signal-to-noise ratio (SNR; at the cost of angular resolution). For the Band 6 observations, during this process, we tested several choices for the pixel size (namely, 0.″05, 0.″075, and 0.″10) and channel width (35, 50, 75, and 100 km s^{-1}), as well as the effect of slightly changing the phase center within a beam size and slightly shifting the velocity of the first channel. The typical sensitivity (rms) of these cubes is equivalent to $1\sigma = 75\ \mu{\rm Jy\ beam^{-1}}$ in $35\ {\rm km\ s^{-1}}$ channels, and they have a typical beam size of $0.''36 \times 0.''28$. As described below, all of these data cubes are used to robustly estimate the uncertainties on the line parameters.

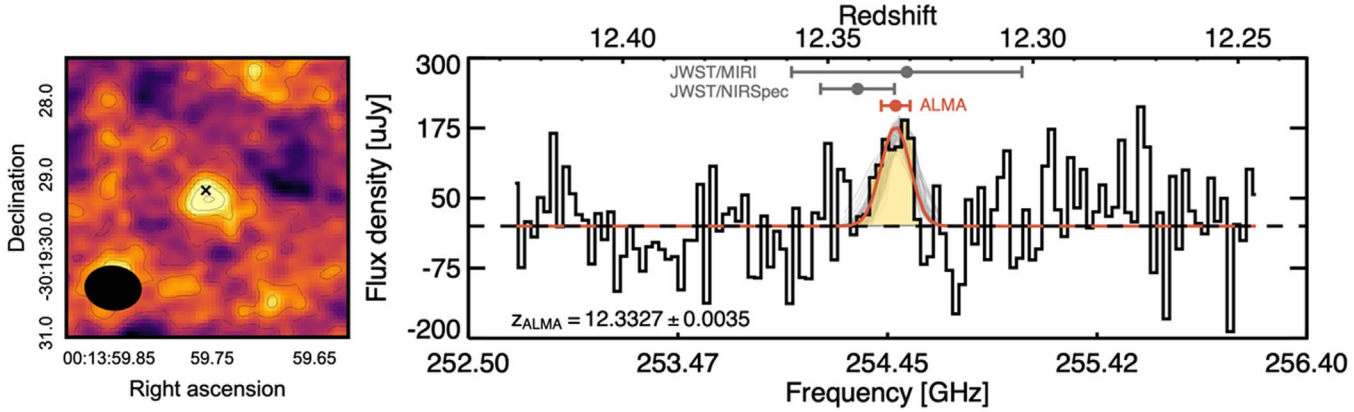

Figure 1. *Detection of the [OIII] 88 μm transition at z = 12.3.* The left panel shows the 3.″5 × 3.″5 moment-0 map of the line, along with the ALMA beam size (black ellipse) and the JWST NIRCam position of GHZ2 (black cross). Contours show SNR in steps of ±1σ (with dashed lines for negative values). The ∼5σ detection from ALMA is in very good agreement with the JWST position. The extracted spectrum from the peak pixel is shown on the right panel along with the best-fit Gaussian function (red solid line) and associated uncertainty (gray lines; see the main text for details), implying a spectroscopic redshift of $z = 12.3327 \pm 0.0035$. On the top, we show the associated redshifts inferred from the different instruments, including NIRSpec, MIRI, and ALMA. Thanks to the higher spectral resolution of the ALMA observations, the redshift precision is increased by ∼5×.

In the case of the Band 8 observations, the achieved 1σ rms is around 500 μJy beam^{-1} in 35 km s^{-1} channels, with a beam size of 0.″36 × 0.″32.

2.2. The [O III]88 μm Transition at z = 12.3: Line Properties

We use the collection of data cubes described above to search for the [O III] 88 μm emission line using an iterative process as follows. First, we extract the spectrum from each data cube exactly at the JWST position of GHZ2. Second, we identify the brightest channel within the expected frequency range of the redshifted [O III]88 μm line base on the JWST/MIRI and JWST/NIRSpec spectroscopic redshifts and perform a Gaussian fit with A, σ, and $\nu_{\rm cent}$ as free parameters (with a flat zero continuum). Then, to improve the SNR of each extracted spectrum, we create a moment-0 map by collapsing the data cube within the FWHM of the best-fit Gaussian function and reextract the spectrum but now at the position of the peak pixel in this moment-0 map. Finally, we perform a new Gaussian fit around the expected frequency and save the best-fit parameters. Reassuringly, all the extracted spectra (those extracted at the JWST position and at the peak ALMA pixel) identify the same feature as an emission line with a significance of ≈4.5−5.2σ, confirming the tentative detection reported in J. A. Zavala et al. (2024).

Figure 1 shows the extracted spectrum and associated moment-0 map (right and left panels, respectively) along with the adopted best-fit Gaussian function (red solid line). The best-fit Gaussian functions from other spectra are also shown to illustrate the typical variance in the data (gray lines). The fiducial line properties and associated uncertainties are assumed to be the median values of all the different best-fit functions and their standard deviation. This approach allows us to properly take into account the impact of the imaging parameters in the shape of the line and to robustly estimate the uncertainties in the best-fit values. These best-fit properties are summarized in Table 1.

2.3. An Upper Limit on the [O III] 52 μm Line Luminosity

Armed with a more precise spectroscopic redshift from the [O III] 88 μm detection, we search for the 52 μm line around the expected frequency of 433.96 GHz, but no obvious line was detected (see the Appendix). We estimate an upper limit on the [O III] 52 μm line luminosity using the measured local noise rms, adopting the [O III] 88 μm line width of 186 ± 58 km s^{-1} (see Table 1) and assuming no spatially extended emission beyond the beam size. This results in a 3σ upper limit of $L_{\rm [O\,III]52\,\mu m} < 9.6 \times 10^8\,L_\odot$, implying a 3σ upper limit on the 52–88 μm line ratio of $L_{\rm [O\,III]52\,\mu m}/L_{\rm [OIII]88\,\mu m} < 5.6$.

Table 1
[O III] 88 μm Line Properties (Uncorrected for Gravitational Amplification)

GHZ2	
R.A. = 00:13:59.76; Decl. = −30:19:29.16	
$z_{\rm [O\,III]88\,\mu m}$	12.3327 ± 0.0035
$z_{\rm NIRSpec}$[a]	12.342 ± 0.009
$z_{\rm MIRI}$[b]	12.33 ± 0.04
$\nu_{\rm cent}$ [GHz]	254.487 ± 0.019
FWHM [km s^{-1}]	186 ± 58
$S_{\rm total}$ [mJy km s^{-1}]	36 ± 10
$L_{\rm [O\,III]}$ [$L_\odot$] × 10^8	1.7 ± 0.4

Notes.
[a] M. Castellano et al. (2024).
[b] J. A. Zavala et al. (2024).

3. Results

3.1. Detection of [O III] 88 μm: Expectations and Implications

Using observations of local and low-redshift galaxies with the Herschel Space Observatory, I. De Looze et al. (2014) found a set of correlations between the [O III] 88 μm line luminosity and galaxies' star formation rate (SFR) for different galaxy populations. Evolved, massive star-forming galaxies (referred as *starbursts* in the aforementioned work) and composite/AGN systems are clearly offset from metal-poor star-forming dwarf galaxies. These correlations seems to be valid at $z \sim 5$–9, as can be seen in Figure 2, where we plot all the high-redshift [O III] 88 μm detections to date. Lyman break galaxies (LBGs) and Lyα emitters (LAEs) follow the same local relation found for metal-poor dwarf galaxies, while QSO and submillimeter-selected galaxies are in better agreement with the local relation for composite/AGN (although with large

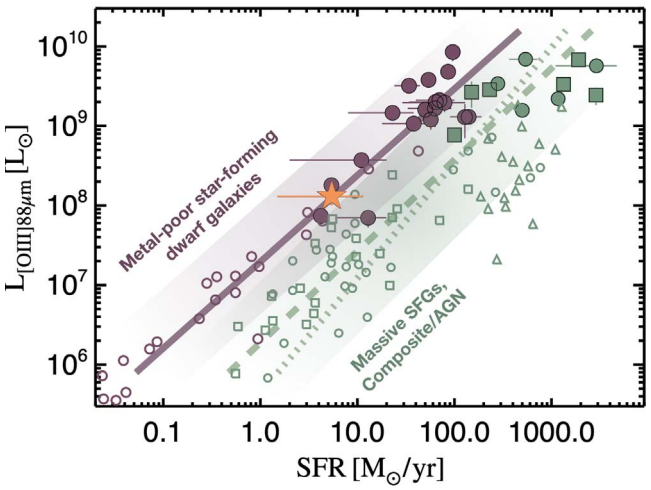

Figure 2. *The SFR–[O III] line luminosity relationship.* The open symbols represent the sample of low-redshift ($z \lesssim 0.3$) galaxies presented in I. De Looze et al. (2014), with purple circles representing metal-poor "dwarf" galaxies, green open circles for more massive star-forming galaxies, green open squares for composite/AGN, and green open triangles for ultraluminous infrared galaxies. The relationships derived by I. De Looze et al. (2014) are also plotted as solid, dashed, and dotted lines for the population of metal-poor "dwarf" galaxies, star-forming galaxies, and composite/AGN, respectively. Solid symbols represent high-redshift galaxies ($z \approx 5$–9; as compiled in H. S. B. Algera et al. 2024 and T. J. L. C. Bakx et al. 2024), with purple circles for LBGs/LAEs, green circles for submillimeter galaxies, and green squares for QSOs. Our target, GHZ2, is represented by the yellow star (adopting the range of SFRs from J. A. Zavala et al. 2024 and correcting from magnification), and along with other high-z LBGs, it nicely follows the local relationship for metal-poor "dwarf" galaxies. Note that the metallicity of GHZ2 is constrained to be $Z \approx 0.05-0.1\ Z_\odot$ (A. Calabro et al. 2024; M. Castellano et al. 2024; J. A. Zavala et al. 2024).

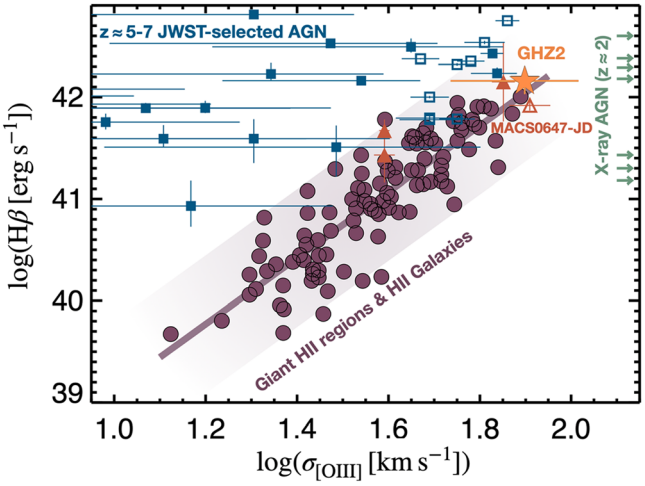

Figure 3. *The* Hβ *line luminosity–velocity dispersion relationship.* The position of GHZ2 in the L–σ relationship for Giant H II regions and H II-galaxies is represented by the yellow star (adopting the lensing-corrected $L_{H\beta}$ reported in J. A. Zavala et al. 2024 and the line width from the ALMA [O III] 88 μm detection reported in this work). As can be seen, the $z = 12$ galaxy follows the relation found for H II-galaxies (as reported by J. Melnick et al. 2017; solid purple line and shaded region), suggesting a similar nature for both objects: young burst of star formation. The three orange solid triangles show $z \approx 6$–7 H II-galaxies recently identified (R. Chávez et al. 2024), while the open orange triangle represents MACS0647-JD at $z = 10.2$ (T. Y.-Y. Hsiao et al. 2024b). Finally, we plot the high-redshift AGN sample from A. J. Taylor et al. (2024) and R. Maiolino et al. (2024b) as solid and open squares, respectively, and indicate the position of more massive AGN at $z \sim 2$ (D. Kakkad et al. 2020) with green arrorows. The AGN deviate from the relationship for H II-dominated systems.

scatter and with some objects being consistent with both relationships).

In this context, we show in Figure 2 the [O III] 88 μm line luminosity and SFR measured for our target and compare them with the reported relationships and with previous detections from high-redshift galaxies. We adopt the line luminosity reported above corrected by magnification ($\mu = 1.3$; P. Bergamini et al. 2023) and the range of SFR values reported by J. A. Zavala et al. (2024) based on the spectrophotometric spectral energy distribution (SED) fittings and the Hα line (2–12 $M_\odot$ yr^{-1}, after correcting for magnification).

As can been seen in the figure, GHZ2 lies on a locus comparable to some $z \sim 8$ LBGs/LAEs and in very good agreement with the local relationship for metal-poor dwarf galaxies. These galaxies are dominated by star formation, and thus, by analogy, we suggest that it might also be the case for our $z = 12$ target. Actually, the measured line luminosity is also in broad agreement with the predictions from the SERRA zoom-in simulations for galaxies with similar properties as GHZ2, in terms of SFRs and redshifts (M. Kohandel et al. 2023), which further support the star formation scenario for GHZ2. To further test this interpretation, below we compare other properties of GHZ2 with those measured directly for well-known systems dominated by star formation, such as H II regions and H II galaxies[23] (while the potential contribution of an AGN is discussed in Section 4).

[23] H II galaxies are compact low-mass systems ($M_\star < 10^9\ M_\odot$) whose luminosities are almost completely dominated by a massive recent burst of star formation; see D. Fernández Arenas et al. (2018), A. L. González-Morán et al. (2021), and references therein.

Over the past decades, it has been shown that giant H II regions exhibit a correlation between the luminosity of the Balmer emission lines (typically Hβ) and the line velocity dispersion (R. Terlevich & J. Melnick 1981). Although the physical origin of this relation is still a matter of debate, it is typically thought to be driven by the total mass of the (gravitationally bounded) star-forming region, dominated by young super star clusters. The relation has been calibrated using samples of several dozens of local and extragalactic giant H II regions (e.g., R. Chávez et al. 2014) and shown to be also valid for H II-galaxies up to $z \sim 3$ (e.g., A. L. González-Morán et al. 2021). J. Melnick et al. (2017) presented a new calibration using the [O III] 5007 Å line width and the Hβ line luminosity that shows a similar scatter to the original $L_{H\beta} - \sigma_{H\beta}$ relationship. Here, we use this correlation given that the Balmer lines are not spectrally resolved for our target and test whether GHZ2 follows a similar trend, as expected if the source is dominated by young bursts of star formation and assuming the relationship does not evolve significantly with redshift (note that the $z \sim 6$–7 H II-galaxies recently reported by R. Chávez et al. 2024 follow the same relationship, as can be seen in Figure 3).

We adopt the lensing-corrected Hβ luminosity of $\log L_{H\beta} = 42.16^{+0.09}_{-0.13}$ erg s^{-1} from J. A. Zavala et al. (2024; inferred from the Hα line assuming zero dust attenuation) and the [O III] 88 μm line width provided by the ALMA observations as a proxy for the [O III] 5007Å velocity dispersion (given that both transitions are produced by the same ion and the [O III] 5007 Å line is unresolved in the MIRI low-resolution spectrum). As can be seen in Figure 3, GHZ2 follows the same relationship found for giant H II regions, suggesting that this very high-redshift galaxy is also powered

by (extreme) star formation. Actually, some of the [O III] 88 μm-detected dwarf galaxies described above are also known to harbor bright H II regions powered by super star clusters (S. C. Madden et al. 2013). This might imply that the high-ionization conditions in GHZ2 are likely driven by extreme H II regions associated with young bursts of star formation. The same can be said for the $z = 10.2$ MACS0647-JD galaxy recently observed with NIRSpec and MIRI (T. Y.-Y. Hsiao et al. 2024b, 2024a). This object also follows the relationship derived for H II-dominated systems, which supports the conclusions by T. Y.-Y. Hsiao et al. (2024a) who argued against an AGN-dominated galaxy.

On the other hand, while similar relationships between the Balmer line luminosities and lines' velocity dispersion have been reported for AGN (e.g., L. C. Ho et al. 2003), typical AGN hosting supermassive black holes show emission lines significantly broader than the H II regions and H II galaxies (with [O III] line widths of $>300\,\mathrm{km\,s^{-1}}$; e.g., D. Kakkad et al. 2020). Moreover, while less massive AGN with narrower line widths have recently been found by JWST up to $z \sim 7$ or beyond, they have brighter line luminosities compared to star-forming-dominated systems (see Figure 3). All of this supports our conclusion that GHZ2 is most likely dominated by a burst of star formation.

Given that the population of young, low-metallicity massive clusters powering giant H II regions has been proposed to be progenitor of globular clusters (e.g., L. C. Ho 1997; S. F. Portegies Zwart et al. 2010; E. Terlevich et al. 2018), it is possible that the current starburst episode of GHZ2 might result in the formation of protoglobular clusters or other compact stellar systems. Indeed, its low metallicity and enhanced nitrogen abundance has already been noticed to be consistent with the expected progenitor population for globular clusters (M. Castellano et al. 2024), as well as its high SFR and stellar mass surface densities (Y. Ono et al. 2023; A. Calabro et al. 2024). This might point toward an evolutionary connection between the bright, compact high-redshift galaxies discovered by JWST (including GHZ2) and the enigmatic population of old globular clusters (see also C. Charbonnel et al. 2023; Y. Isobe et al. 2023; M. Castellano et al. 2024; R. Marques-Chaves et al. 2024; M. W. Topping et al. 2024). This is discussed in detail below in Section 4.

3.2. Dynamical Mass

Assuming a spherical geometry (a reasonable assumption for this very compact source), we estimate the dynamical mass using the virial equation (e.g., M. Pettini et al. 2001; J. Wolf et al. 2010):

$$M_{\rm dyn} = \frac{5\sigma^2 R}{G}, \quad (1)$$

where σ is the velocity dispersion and R is the virial radius. The velocity dispersion is determined from the [O III] 88 μm transition ($\sigma = 79 \pm 25\,\mathrm{km\,s^{-1}}$), and the virial radius is adopted to be the half-light radius measured from the JWST/NIRcam images, with reported values of $r_{1/2} = 39 \pm 11$ pc (Y. Ono et al. 2023) and 105 ± 9 pc (L. Yang et al. 2022). Using Equation (1) and the aforementioned assumptions, we constrain the dynamical mass to be $3 \times 10^8 - 8 \times 10^8\,M_\odot$.

This is remarkably similar to the stellar masses inferred from the spectrophotometric SED fitting analysis presented in J. A. Zavala et al. (2024), with best-fit stellar masses of $2 \times 10^8 - 8 \times 10^8\,M_\odot$ (assuming a magnification of $\mu = 1.3$; P. Bergamini et al. 2023). This implies a dynamical-to-stellar mass ratio of close to unity for GHZ2, similar to the measured values for globular clusters (e.g., D. A. Forbes et al. 2014), providing more evidence for a relation between these objects as discussed below.

Finally, to assess the impact of our assumptions on the inferred dynamical mass, we alternatively use the approach described by H. Übler et al. (2023). Here, we assume Sérsic indices of $n = 1$ and 1.5, with axis ratios in the range of $q = \{0.3 : 0.7\}$. Overall, the dynamical masses inferred from these models fall within the range of the values described above but allow for up to a 50% increase. However, given the compactness and symmetry of the source (T. Treu et al. 2023), we adopt the mass constraints from the virial equation described above as our fiducial value.

3.3. Constraining the Electron Density

The [O III] 52 μm-over-[O III] 88 μm line luminosity ratio provides strong constraints on the electron density almost independently from metallicity, ionization field effects, or electron temperature (e.g., T. Jones et al. 2020; M. Killi et al. 2023; Y. Nakazato et al. 2023). Here, given the nondetection of the [O III] 52 μm transition (see Section 2.3), we determine a 3σ upper limit on the ionized oxygen electron density of $\log(n_e\,[\mathrm{cm^{-3}}]) < 3.62$ (see Figure 4). While this value seems high compared to the typical values found in star-forming galaxies at low redshifts ($\sim 100\,\mathrm{cm^{-3}}$; e.g., M. Kaasinen et al. 2017), this upper limit is totally consistent with the measured electron densities of high-redshift ($z \gtrsim 5$) star-forming galaxies and with the apparent redshift evolution of n_e (e.g., Y. Isobe et al. 2023; G. C. Jones et al. 2024), particularly when combined with the lower limit of $n_e \gtrsim 100\,\mathrm{cm^{-3}}$ reported in J. A. Zavala et al. (2024). On the other hand, the electron density of GHZ2 contrasts with that of GNz11, the brightest confirmed galaxy at $z > 10$. In the case of GNz11, the [N IV] doublet and N III] multiplet indicate extremely large electron densities ($>10^5\,\mathrm{cm^{-3}}$) in better agreement with the broad line regions in AGN (R. Maiolino et al. 2024a). We stress, however, that transitions with different ionization potentials might trace different regions of the interstellar medium with different electron densities (e.g., X. Ji et al. 2024).

4. Discussion

4.1. A System Dominated by Star Formation

The nature of the intriguing population of bright, high-redshift galaxies discovered by JWST remains unclear. What processes drive their high luminosity so early in the Universe's history? Understanding whether these galaxies are dominated by stellar processes or AGN activity is crucial for developing a comprehensive picture of galaxy formation in the early Universe.

In the case of GHZ2, this question has been approached from different perspectives, starting with its JWST/NIRCam morphology. Y. Ono et al. (2023) found that while the source is very compact, it is spatially resolved with a half-light radius of a few tens of parsecs (see also L. Yang et al. 2022). This provides evidence against an AGN-dominated system, although it does not totally rule out some fractional contribution to its continuum luminosity. Similarly, J. A. Zavala et al. (2024), who

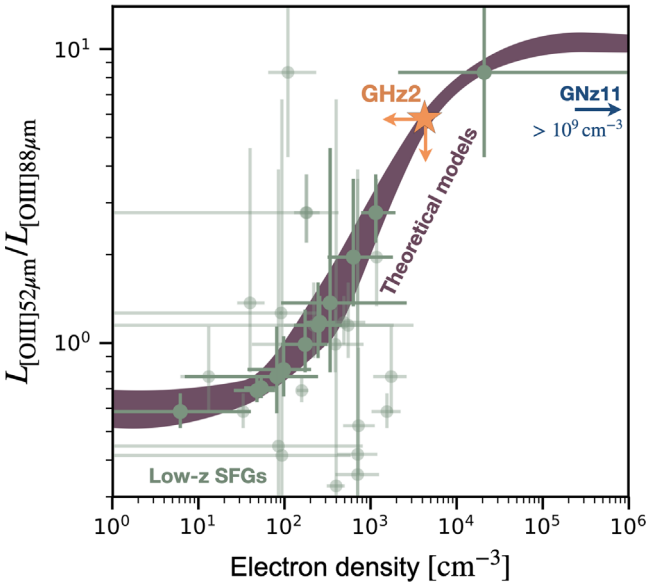

Figure 4. *Constraints on the oxygen electron density.* Predicted 52–88 μm luminosity ratio as a function of electron density generated using PYNEB (V. Luridiana et al. 2015). This ratio is nearly independent to gas temperature, ionization parameter, and metallicity. The 3σ upper limit from our observations (orange star) rules out high-density environments, such as those found in GNz-11 ($>10^9$ cm^{-3}). The comparison data come from the PACS and SPIRE spectrometry of nearby star-forming galaxies (J. A. Fernández-Ontiveros et al. 2016). The solid green symbols indicate the oxygen-derived electron densities, which accurately follow the theoretical predictions, while the semitransparent symbols indicate complementary probes of the electron densities (using [N II] 205/122, [S III] 33/18, and [Ne V] 24/14 ratios). As can be seen, star-forming galaxies show moderate electron densities, consistent with the inferred limit for GHZ2.

presented the detection of Hα and [O III] 5007 Å in a JWST/MIRI spectrum and a spectrophotometric SED analysis of this source, attributed its high luminosity to the presence of a very young, massive, and metal-poor stellar population; but, again, the possibility of having some contribution from AGN remained open. This latter scenario was revitalized given the detection of relatively high-ionization UV transitions and line ratios, and lines with high equivalent widths in the JWST/NIRSpec spectrum presented by M. Castellano et al. (2024), indicating ionizing photons with energies in excess of ~50−60 eV. Nevertheless, the absence of higher ionization lines typically seen in AGN (like He II or [Ne IV] 2424 Å) and the strong upper limit on the [Ne IV]/N IV] ratio put some doubts on this scenario and led the authors to suggest that GHZ2 is most likely dominated by (extreme) star formation. Finally, A. Calabro et al. (2024) presented a comprehensive analysis of the (rest-frame) UV and optical line ratios, finding very high-ionization conditions but indistinguishable between those produced by AGN and low-metallicity, compact star-forming regions.

It is thus clear that GHZ2 shows extreme properties with high-ionization conditions, but a pure AGN model would fail to reproduce all the characteristics described above (such as the lack of some specific atomic transitions and extended emission). Additionally, in Section 3.1 we have shown that this source follows the SFR–[O III] 88 μm relationship found for metal-poor star-forming galaxies and the L–σ relation found for giant H II regions and H II-galaxies, which would be hard to explain within the AGN framework. The fact that the Hα-based SFR is in good agreement (within a factor of ~2) with the star-forming SED modeling (see J. A. Zavala et al. 2024) might also imply that the contribution from AGN (if any) should be low. The same could be said of the fact that the stellar mass (from the SED analysis) and the dynamical mass (from the [O III] 88 μm detection) are consistent with a factor of ~2. Such results would be entirely coincidental in the case of an AGN-dominated system. Finally, the electron density upper limit of $n_e < 4.2 \times 10^3$ cm^{-3}, although high, has been shown to be within the realm of star-forming galaxies (see Section 3.3) and significantly below the typical values of the broad line region in AGN. Hence, we conclude that GHZ2 is most likely dominated by star formation activity driven by metal-poor and young stellar populations.

Furthermore, given its high Hα and Hβ luminosities—consistent only with the most luminous starbursts and H II galaxies (e.g., L. C. Ho et al. 1997; D. Fernández Arenas et al. 2018)—and its remarkable compactness and concentration (Y. Ono et al. 2023; T. Treu et al. 2023), it would be expected that this extreme star formation activity is taking place in the form of super star clusters, commonly found in starburst systems (L. C. Ho et al. 1997). The high specific SFR of GHZ2 of sSFR ≈ 10–30 Gyr^{-1} might actually be evidence of a starburst-like star formation mode propitious to the formation of these massive clusters. This is also supported by the high *burstiness* found for the SERRA-simulated galaxies that match other properties of GHZ2 (A. Pallottini et al. 2022).

However, it is important to remark that, although the star-forming scenario seems the most plausible to explain the nature of this object, available models fail to reproduce the extremely high equivalent widths of the UV lines, some of them only compatible with AGN or composite emission models, as discussed in detail by M. Castellano et al. (2024) and A. Calabro et al. (2024).

4.2. The Progenitor of a Compact Stellar Object

Will GHZ2 evolve into a globular cluster? The fact that GHZ2 might be powered by massive star clusters does not necessarily make it a globular cluster progenitor. However, here we provide additional arguments that might support this scenario and that might, additionally, explain some of the long-standing problems associated with globular clusters.

First, its low metallicity and enhanced nitrogen abundance (M. Castellano et al. 2024) resemble the well-known chemical anomalies observed in globular clusters (e.g., R. D. Cannon et al. 1998)—though not exclusive to them. These abundance patterns are thought to be the product of massive stars in very dense environments (e.g., G. H. Smith 2006), and interestingly, in GHZ2, the presence of very massive stars has been inferred from its high-ionization conditions (A. Calabro et al. 2024; M. Castellano et al. 2024; J. A. Zavala et al. 2024). Moreover, its compact morphology implies a high mass density (with $\Sigma_\star \sim 10^4\, M_\odot$ pc^{-2} and $n_e \approx 100$–4000 cm^{-3}), similar to those found in globular clusters (see Figure 5). In addition, spectrophometric SED fitting analysis on GHZ2 indicates a bursty star formation history for this object (J. A. Zavala et al. 2024; see also Y. Harikane et al. 2024). These short bursts with duration in the range of a few or a few tens of Myr, in combination with its very rapid metal enrichment,[24] would naturally explain the

[24] Note that, despite its young age, GHZ2 shows already a metallicity of $Z \approx 5\%$–$10\%\ Z_\odot$; (A. Calabro et al. 2024; M. Castellano et al. 2024; J. A. Zavala et al. 2024).

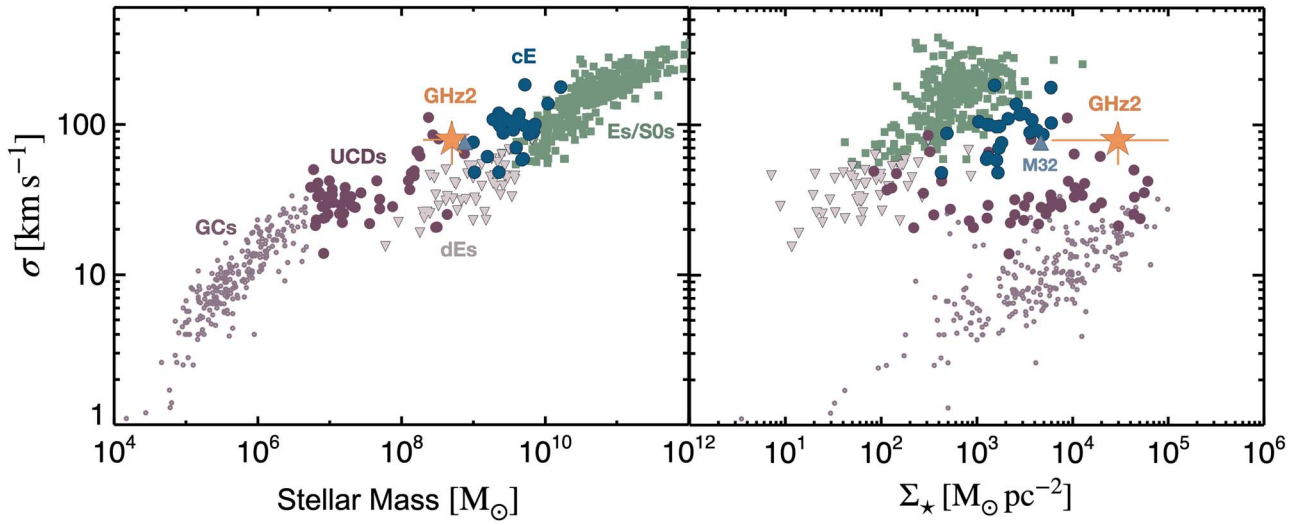

Figure 5. *The stellar mass–velocity dispersion relationship.* The velocity dispersion as a function of stellar mass (left) and stellar mass surface density (right) for different populations of pressure-supported systems (taken from M. A. Norris et al. 2014), including globular clusters (light-purple circles), UCDs (solid purple circles), dwarf ellipticals (down-pointing triangles), compact ellipticals (blue solid circles), and elliptical and S0 galaxies (green squares). Our target, GHZ2, represented by the yellow star, shows a similar stellar mass surface density as globular clusters but with a higher total stellar mass that is in better agreement with those of UCDs and compact ellipticals. Indeed, it occupies a similar locus as M32, the prototypical compact elliptical galaxy (represented by the up-pointing blue triangle). Note, however, that significant mass losses are expected due to stellar and dynamical evolution that would eventually affect the position of GHZ2 on this parameter space.

low spread in stellar ages and the multiple stellar populations observed in globular clusters (see reviews by R. G. Gratton et al. 2012, D. A. Forbes et al. 2018). Lastly, its unique spectral features with UV lines with high EWs and clear emission of the O III 3123 Å fluorescence line[25] (M. Castellano et al. 2024) might be explained by the *stellar exotica* in globular clusters (e.g., X-ray binaries and blue stragglers; S. F. Portegies Zwart et al. 2010) and their high helium abundance (J. E. Norris 2004; F. D'Antona et al. 2005).

There is one thing, however, that appears to be at odds with expected protoglobular cluster properties: the high total mass of GHZ2. With a stellar mass of $\approx 10^8$–$10^9\,M_\odot$ (see Section 3.2), GHZ2 exceeds by more than 1 order of magnitude the masses of even the most massive known globular clusters (see Figure 5). These two values might be reconciled by assuming significant mass losses due to stellar and dynamical evolution (e.g., J. J. Webb & N. W. C. Leigh 2015), but even assuming extreme values, GHZ2 would only be barely consistent with the most massive population of globular clusters. Alternatively, this tension might be solved by the models presented in A. D'Ercole et al. (2008), in which most of the first-generation stars are lost due to the expansion and stripping of the cluster's outer layers caused by the heating from supernova ejecta, followed by a highly concentrated second generation of stars. Indeed, several models require this first generation to be at least ∼10 times more massive than current globular cluster survivors in order to explain the different chemical composition of the multiple stellar populations (e.g., A. Renzini et al. 2015).

Another possibility is that GHZ2 hosts an ensemble of super star clusters. This scenario is supported not only by its large mass but also by its size. Its effective radius of ∼40–100 pc exceeds by a factor from a few to tens the sizes of the few high-redshift protoglobular clusters that have been individually resolved thanks to strong gravitational lensing effects (e.g., E. Vanzella et al. 2023; A. Adamo et al. 2024). These two discrepancies (the size and total mass) could be solved by assuming that GHZ2 is actually a superposition of several individual clusters (e.g., A. Adamo et al. 2024; L. Mowla et al. 2024). Supporting evidence for this scenario is found in the simulations presented in M. Kohandel et al. (2023), in which the [O III] 88 μm emission of $z > 10$ galaxies is resolved into several individual H II regions. Moreover, although it is possible that these H II regions might be normal OB associations with a high probability of dissolution, as discussed above and in Section 4.1, GHZ2 shows properties rather similar to those of massive super star clusters.

The final scenario discussed considers the possibility that GHZ2 is an ultracompact dwarf (UCD) galaxy (e.g. C. Maraston et al. 2004) or a protocompact elliptical given the similarities between their stellar mass, size, and velocity dispersion (see Figure 5). The formation processes of these objects remains unclear, but they are known to bridge the gap between stellar clusters and galaxies (e.g., M. A. Norris et al. 2014; E. Terlevich et al. 2018; see also Figure 5), and it has been shown that some of these objects could represent the massive end of the globular cluster luminosity function (e.g., S. Mieske et al. 2012) or the result of merging of several star clusters (e.g., F. Urrutia Zapata et al. 2019). While it is also true that some UCDs show an elevated dynamical-to-stellar mass ratio that can be attributed to the presence of massive black holes (e.g., A. C. Seth et al. 2014), GHZ2 shows a dynamical-to-stellar mass ratio around 1 (see Section 3.2), in better agreement with globular clusters and compact ellipticals (D. A. Forbes et al. 2014).

We thus conclude that GHZ2 might be powered by young and compact star-forming regions that could evolve into globular clusters or to become the central core of a more massive galaxy. This is, however, only suggestive and not conclusive. Further observations and simulations should be conducted to further test this interpretation.

[25] This transition is pumped by photons emitted from singly ionized helium atoms; i.e., He II Lyα photons at $\lambda_{\rm rest} = 303.78$ Å.

5. Summary

Through the detection of [O III] 88 μm at $z = 12.33$, we have demonstrated the feasibility of studying the early ($z > 10$) Universe with ALMA and its unique synergy with JWST to characterize the most distant galaxies known to date. By combining these observations with previous multiwavelength photometry and spectroscopy, we investigated the nature of GHZ2—one of the brightest known galaxies in the $z > 10$ Universe, just 350 million years after the Big Bang. We concluded that this object is likely powered by young bursts of star formation similar to those found in giant H II regions (metal-poor, massive, and compact star clusters). Finally, we presented compelling evidence suggesting that GHZ2 might be a progenitor of globular clusters or represent the early phases of a compact dwarf or elliptical galaxy. While this characterization is very suggestive, further observations with both high spectral and high angular resolution are needed to test this hypothesis and to fully understand some of the unique properties of this object.

Acknowledgments

We thank Stefano Carniani, Mahsa Kohandel, and Andrea Ferrara for the stimulating discussions; Angela Adamo, Hiddo Algera, Ricardo Chavez, and Anthony Taylor for sharing their data sets; and Takuya Hashimoto and Yurina Nakazato for sharing information about their research projects. J.A.Z. acknowledges funding from JSPS KAKENHI grant No. KG23K13150. M.C. and P.S. acknowledge INAF Mini Grant 2022 "Reionization and Fundamental Cosmology with High-Redshift Galaxies," INAF Mini Grant 2022 "The evolution of passive galaxies through cosmic time," and PRIN 2022 MUR project 2022CB3PJ3—First Light And Galaxy aSsembly (FLAGS) funded by the European Union—Next Generation EU. L.C.H. was supported by the National Science Foundation of China (11991052, 12233001), the National Key R&D Program of China (2022YFF0503401), and the China Manned Space Project (CMS-CSST-2021-A04, CMS-CSST-2021-A06). P.G.P.-G. acknowledges support from grant PID2022-139567NB-I00 funded by the Spanish Ministerio de Ciencia, Innovación y Universidades MICIU/AEI/10.13039/501100011033 and the European Union FEDER program *Una manera de hacer Europa*. This Letter makes use of the following ALMA data: ADS/JAO.ALMA#2021.A.00020.S and JAO.ALMA#2023.A.00017.S. ALMA is a partnership of ESO (representing its member states), NSF (USA), and NINS (Japan), together with NRC (Canada), MOST, ASIAA (Taiwan), and KASI (Republic of Korea), in cooperation with the Republic of Chile. The Joint ALMA Observatory is operated by ESO, AUI/NRAO, and NAOJ.

Facility: ALMA (Band 6 and Band 8; G. A. Ediss et al. 2004; Y. Sekimoto et al. 2008), JWST (J. P. Gardner et al. 2006, 2023)

Software: CASA (CASA Team et al. 2022),

Appendix
Band 8 Spectrum Around the [O III] 52 μm Transition

Figure 6 shows the extracted spectrum at the position of GHZ2 (right panel) along with a collapsed data cube within the expected FWHM of the line (from approx. 433.8 to 434.1 GHz; left panel). The line is undetected at the current depth of the observations but provides useful constraints on the electron density, as discussed in Section 3.3.

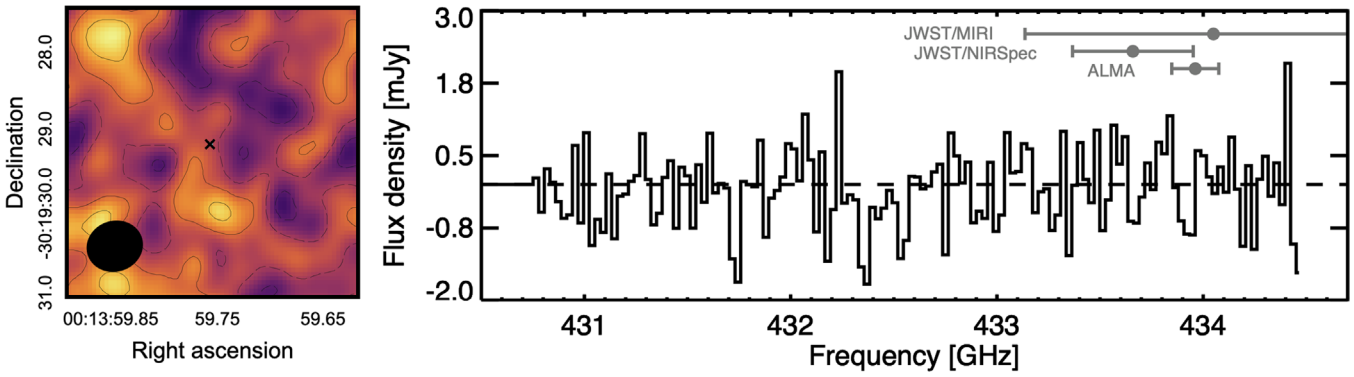

Figure 6. *ALMA Band 8 spectrum covering the [O III] 52 μm transition at $z \approx 12.3$.* Analog to Figure 1 but for the 52 μm observations. The left panel shows a $3\farcs5 \times 3\farcs5$ image of the collapsed data cube within the expected FWHM of the line (based on the [O III] 88 μm detection). Nevertheless, there is no significant detection around the position of GHZ2 (black cross). Contours show $\pm 1\sigma$ and $\pm 2\sigma$, with dashed lines for negative values. The extracted spectrum at the position of the source is shown on the right panel along with the redshift constraints from the different instruments.

ORCID iDs

Jorge A. Zavala https://orcid.org/0000-0002-7051-1100
Ikki Mitsuhashi https://orcid.org/0000-0001-7300-9450
Marco Castellano https://orcid.org/0000-0001-9875-8263
Hollis Akins https://orcid.org/0000-0003-3596-8794
Veronique Buat https://orcid.org/0000-0003-3441-903X
Caitlin M. Casey https://orcid.org/0000-0002-0930-6466
David Fernandez-Arenas https://orcid.org/0000-0002-6874-4570
Maximilien Franco https://orcid.org/0000-0002-3560-8599
Adriano Fontana https://orcid.org/0000-0003-3820-2823
Luis C. Ho https://orcid.org/0000-0001-6947-5846
Ryota Ikeda https://orcid.org/0000-0002-2634-9169
Anton M. Koekemoer https://orcid.org/0000-0002-6610-2048
Jed McKinney https://orcid.org/0000-0002-6149-8178
Lorenzo Napolitano https://orcid.org/0000-0002-8951-4408
Paola Santini https://orcid.org/0000-0002-9334-8705
Stephen Serjeant https://orcid.org/0000-0002-0517-7943
Roberto Terlevich https://orcid.org/0000-0001-6774-3499
L. Y. Aaron Yung https://orcid.org/0000-0003-3466-035X

References

Adamo, A., Bradley, L. D., Vanzella, E., et al. 2024, Natur, 632, 513
Adams, N. J., Conselice, C. J., Austin, D., et al. 2024, ApJ, 965, 169
Algera, H. S. B., Inami, H., Sommovigo, L., et al. 2024, MNRAS, 527, 6867
Álvarez-Márquez, J., Colina, L., Crespo Gómez, A., et al. 2024, A&A, 686, A85
Arrabal Haro, P., Dickinson, M., Finkelstein, S. L., et al. 2023, Natur, 622, 707
Bakx, T. J. L. C., Algera, H. S. B., Venemans, B., et al. 2024, MNRAS, 532, 2270
Bakx, T. J. L. C., Tamura, Y., Hashimoto, T., et al. 2020, MNRAS, 493, 4294
Bakx, T. J. L. C., Zavala, J. A., Mitsuhashi, I., et al. 2023, MNRAS, 519, 5076
Bergamini, P., Acebron, A., Grillo, C., et al. 2023, ApJ, 952, 84
Boylan-Kolchin, M. 2023, NatAs, 7, 731
Bunker, A. J., Saxena, A., Cameron, A. J., et al. 2023, A&A, 677, A88
Calabro, A., Castellano, M., Zavala, J. A., et al. 2024, ApJ, 975, 245
Cannon, R. D., Croke, B. F. W., Bell, R. A., Hesser, J. E., & Stathakis, R. A. 1998, MNRAS, 298, 601
Carniani, S., D'Eugenio, F., Ji, X., et al. 2024a, arXiv:2409.20533
Carniani, S., Hainline, K., D'Eugenio, F., et al. 2024b, Natur, 633, 318
Carniani, S., Maiolino, R., Pallottini, A., et al. 2017, A&A, 605, A42
CASA Team, Bean, B., Bhatnagar, S., et al. 2022, PASP, 134, 114501
Castellano, M., Fontana, A., Treu, T., et al. 2022, ApJL, 938, L15
Castellano, M., Fontana, A., Treu, T., et al. 2023, ApJL, 948, L14
Castellano, M., Napolitano, L., Fontana, A., et al. 2024, ApJ, 972, 143
Charbonnel, C., Schaerer, D., Prantzos, N., et al. 2023, A&A, 673, L7
Chávez, R., Terlevich, R., Terlevich, E., et al. 2014, MNRAS, 442, 3565
Chávez, R., Terlevich, R., Terlevich, E., et al. 2024, arXiv:2404.16261
Curtis-Lake, E., Carniani, S., Cameron, A., et al. 2023, NatAs, 7, 622
D'Antona, F., Bellazzini, M., Caloi, V., et al. 2005, ApJ, 631, 868
De Looze, I., Cormier, D., Lebouteiller, V., et al. 2014, A&A, 568, A62
D'Ercole, A., Vesperini, E., D'Antona, F., McMillan, S. L. W., & Recchi, S. 2008, MNRAS, 391, 825
Ediss, G. A., Carter, M., Cheng, J., et al. 2004, in Fifteenth Int. Symp. Space Terahertz Technology, ed. G. Narayanan, 181
Feldmann, R., Boylan-Kolchin, M., Bullock, J. S., et al. 2024, arXiv:2407.02674
Fernández Arenas, D., Terlevich, E., Terlevich, R., et al. 2018, MNRAS, 474, 1250
Fernández-Ontiveros, J. A., Spinoglio, L., Pereira-Santaella, M., et al. 2016, ApJS, 226, 19
Ferrara, A., Pallottini, A., & Dayal, P. 2023, MNRAS, 522, 3986
Finkelstein, S. L., Bagley, M. B., Ferguson, H. C., et al. 2023, ApJL, 946, L13
Forbes, D. A., Bastian, N., Gieles, M., et al. 2018, RSPSA, 474, 20170616
Forbes, D. A., Norris, M. A., Strader, J., et al. 2014, MNRAS, 444, 2993
Fujimoto, S., Arrabal Haro, P., Dickinson, M., et al. 2023, ApJL, 949, L25
Gardner, J. P., Mather, J. C., Abbott, R., et al. 2023, PASP, 135, 068001
Gardner, J. P., Mather, J. C., Clampin, M., et al. 2006, SSRv, 123, 485
González-Morán, A. L., Chávez, R., Terlevich, E., et al. 2021, MNRAS, 505, 1441
Gratton, R. G., Carretta, E., & Bragaglia, A. 2012, A&ARv, 20, 50
Harikane, Y., Inoue, A. K., Ellis, R. S., et al. 2024, arXiv:2406.18352
Hashimoto, T., Inoue, A. K., Mawatari, K., et al. 2019, PASJ, 71, 71
Hegde, S., Wyatt, M. M., & Furlanetto, S. R. 2024, JCAP, 08, 025
Ho, L. C. 1997, RMxAA, 6, 5
Ho, L. C., Filippenko, A. V., & Sargent, W. L. W. 1997, ApJ, 487, 579
Ho, L. C., Filippenko, A. V., & Sargent, W. L. W. 2003, ApJ, 583, 159
Hsiao, T. Y.-Y., Abdurro'uf, A., Coe, D., et al. 2024a, ApJ, 973, 8
Hsiao, T. Y.-Y., Álvarez-Márquez, J., Coe, D., et al. 2024b, ApJ, 973, 81
Inoue, A. K., Shimizu, I., Tamura, Y., et al. 2014, ApJL, 780, L18
Inoue, A. K., Tamura, Y., Matsuo, H., et al. 2016, Sci, 352, 1559
Isobe, Y., Ouchi, M., Tominaga, N., et al. 2023, ApJ, 959, 100
Ji, X., Übler, H., Maiolino, R., et al. 2024, MNRAS , 535, 881
Jones, G. C., Bunker, A. J., Telikova, K., et al. 2024, arXiv:2405.12955
Jones, T., Sanders, R., Roberts-Borsani, G., et al. 2020, ApJ, 903, 150
Kaasinen, M., Bian, F., Groves, B., Kewley, L. J., & Gupta, A. 2017, MNRAS, 465, 3220
Kaasinen, M., van Marrewijk, J., Popping, G., et al. 2023, A&A, 671, A29
Kakkad, D., Mainieri, V., Vietri, G., et al. 2020, A&A, 642, A147
Katz, H., Galligan, T. P., Kimm, T., et al. 2019, MNRAS, 487, 5902
Killi, M., Watson, D., Fujimoto, S., et al. 2023, MNRAS, 521, 2526
Kohandel, M., Ferrara, A., Pallottini, A., et al. 2023, MNRAS, 520, L16
Liu, B., & Bromm, V. 2022, ApJL, 937, L30
Luridiana, V., Morisset, C., & Shaw, R. A. 2015, A&A, 573, A42
Madden, S. C., Rémy-Ruyer, A., Galametz, M., et al. 2013, PASP, 125, 600
Maiolino, R., Scholtz, J., Curtis-Lake, E., et al. 2024b, A&A, 691, A145
Maiolino, R., Scholtz, J., Witstok, J., et al. 2024a, Natur, 627, 59
Maraston, C., Bastian, N., Saglia, R. P., et al. 2004, A&A, 416, 467
Marques-Chaves, R., Schaerer, D., Kuruvanthodi, A., et al. 2024, A&A, 681, A30
Melnick, J., Telles, E., Bordalo, V., et al. 2017, A&A, 599, A76
Mieske, S., Hilker, M., & Misgeld, I. 2012, A&A, 537, A3
Mowla, L., Iyer, K., Asada, Y., et al. 2024, arXiv:2402.08696
Naidu, R. P., Oesch, P. A., van Dokkum, P., et al. 2022, ApJL, 940, L14
Nakazato, Y., Yoshida, N., & Ceverino, D. 2023, ApJ, 953, 140
Norris, J. E. 2004, ApJL, 612, L25
Norris, M. A., Kannappan, S. J., Forbes, D. A., et al. 2014, MNRAS, 443, 1151
Ono, Y., Harikane, Y., Ouchi, M., et al. 2023, ApJ, 951, 72
Pallottini, A., Ferrara, A., Gallerani, S., et al. 2022, MNRAS, 513, 5621
Pettini, M., Shapley, A. E., Steidel, C. C., et al. 2001, ApJ, 554, 981
Popping, G. 2023, A&A, 669, L8
Portegies Zwart, S. F., McMillan, S. L. W., & Gieles, M. 2010, ARA&A, 48, 431
Renzini, A., D'Antona, F., Cassisi, S., et al. 2015, MNRAS, 454, 4197
Roberts-Borsani, G., Treu, T., Shapley, A., et al. 2024, arXiv:2403.07103
Sanders, R. L., Shapley, A. E., Topping, M. W., Reddy, N. A., & Brammer, G. B. 2023, ApJ, 955, 54
Schouws, S., Bouwens, R. J., Ormerod, K., et al. 2024, arXiv:2409.20549
Sekimoto, Y., Iizuko, Y., Satou, N., et al. 2008, in Ninteenth Int. Symp. Space Terahertz Technology, ed. W. Wild, 253
Seth, A. C., van den Bosch, R., Mieske, S., et al. 2014, Natur, 513, 398
Smith, G. H. 2006, PASP, 118, 1225
Sun, G., Faucher-Giguère, C.-A., Hayward, C. C., et al. 2023, ApJL, 955, L35
Taylor, A. J., Finkelstein, S. L., Kocevski, D. D., et al. 2024, arXiv:2409.06772
Terlevich, E., Fernández-Arenas, D., Terlevich, R., et al. 2018, MNRAS, 481, 268
Terlevich, R., & Melnick, J. 1981, MNRAS, 195, 839
Topping, M. W., Stark, D. P., Senchyna, P., et al. 2024, MNRAS, 529, 3301
Treu, T., Calabrò, A., Castellano, M., et al. 2023, ApJL, 942, L28
Übler, H., Maiolino, R., Curtis-Lake, E., et al. 2023, A&A, 677, A145
Urrutia Zapata, F., Fellhauer, M., Alarcón Jara, A. G., Matus Carrillo, D. R., & Aravena, C. A. 2019, MNRAS, 489, 2746
Vanzella, E., Claeyssens, A., Welch, B., et al. 2023, ApJ, 945, 53
Wang, B., Fujimoto, S., Labbé, I., et al. 2023, ApJL, 957, L34
Webb, J. J., & Leigh, N. W. C. 2015, MNRAS, 453, 3278
Wolf, J., Martinez, G. D., Bullock, J. S., et al. 2010, MNRAS, 406, 1220
Yang, L., Morishita, T., Leethochawalit, N., et al. 2022, ApJL, 938, L17
Yoon, I., Carilli, C. L., Fujimoto, S., et al. 2023, ApJ, 950, 61
Yung, L. Y. A., Somerville, R. S., Finkelstein, S. L., Wilkins, S. M., & Gardner, J. P. 2024, MNRAS, 527, 5929
Zavala, J. A., Castellano, M., Akins, H. B., et al. 2024, NatAs, Advanced Online Publication